Optimizing and Engineering EuSe–$PbSe_{0.78}Te_{0.22}$–EuSe Multiple-Quantum-Well Laser Structures

M. F. Khodr, P. J. McCann, and B. A. Mason

***Abstract*—In this paper, we present a simulation model to optimize and engineer EuSe–$PbSe_{0.78}Te_{0.22}$–EuSe single-quantum-well lasers. We solve for the effects of strong nonparabolicity of the bands on the optimization process. The optical energy confined in the active region is also calculated for multiple-quantum-well (MQW) lasers. The modal gain-current density relation for this structure is obtained for parabolic band and nonparabolic band systems. The relationships between threshold current, cavity length, and mirror reflectivity are obtained for the MQW structure assuming parabolic and nonparabolic band systems. Finally, in addition to a 20% shift in the output lasing energy, it is concluded that the effects of nonparabolicity on the threshold current values are significant for short-cavity lasers and decrease with an increase in the cavity length.**

***Index Terms*— Lead alloys, modeling, quantum-well lasers, semiconductor diodes, spectroscopy.**

I. Introduction

A PRINCIPAL feature of the quantum-well (QW) laser is that a higher gain can be obtained at a given current density than in the bulk materials. This arises partly from higher population inversion at a given carrier density because of the lower quantized density of states, but mostly from the higher carrier density in the QW because of its smaller width. Equally important, however, in determining laser properties are modal gain, a product of the gain in the well and the optical confinement factor, and the ability to collect injected carriers efficiently [1]. These latter factors prevent the improvement of laser performance for arbitrarily thin QW dimensions unless additional design features are added. These design improvements include the use of multiple QW's (MQW) and/or the separate confinement heterostructure (SCH) scheme where optical confinement is provided by a set of optical confinement layers, while carrier confinement occurs in another embedded layer. By controlling the width of the QW's, one can modify the electron and hole wavefunctions. This results in improvement of the laser characteristics, as well as introduction of new concepts to semiconductor optical devices [2]. In addition to being a promising light source for various applications, other optical devices based on QW structures have been proposed and demonstrated, such as optical modulators [3] and optical bistable devices [4].

Quantum-well lasers (QWL's) have existed only since 1977 [5]. Several kinds of QW heterostructure laser diodes have been constructed using materials from the InP–InGaAsP system and the more highly developed AlGaAs–GaAs system. In these systems, continuous room temperature (CW, 300 K) laser operation has been achieved [5]. The progress in the development of lead salt diode lasers has followed the progress in III–V lasers. Lead salt lasers are made up of the IV–VI compounds: PbS, PbSe, SnTe, PbTe, and SnSe [1]. Among the IV–VI compounds, single- or multiple-QW diode lasers have so far been fabricated in the PbEuSeTe–PbTe, PbSnTe–PbSeTe, and PbEuSe–PbSe material systems [6]. At present, the PbEuSeTe QW system attained CW operation (at a 4.4-μm wavelength) up to 175 K, and pulsed operation (at 3.9 μm) up to 270 K [6].

The bandgaps in IV–VI semiconductor materials are quite small and, therefore, the emission is in the middle and far infrared (IR). Moreover, both the energy gap and the refractive index of lead salts are highly dependent on temperature. Thus, by controlling the temperature, the emission wavelength can be varied. This provides a tunable laser source in the infrared, a source which has found extensive use in ultrahigh-resolution spectroscopy. Lead salt lasers are also used in other applications, such as local oscillators in heterodyne systems [1]. Moreover, it appears that these devices will continue to maintain a significant advantage over II–VI and III–V compound diode lasers for wavelengths of about 3–30 μm at significantly higher temperatures [6]. Finally, individual mid-IR III–V quantum cascade (QC) lasers cannot be easily tuned, and this compromises their use in spectroscopy applications. Higher power emission is presently the only feature where QC lasers are better than IV–VI semiconductor lasers, but this is not a critical parameter for spectroscopy applications since mid-IR detectors are sufficiently sensitive. For these reasons, along with over 20 years of proven performance in various spectroscopy applications, IV–VI semiconductor lasers should continue to be the preferred devices for mid-IR laser spectroscopy.

The above QW structures were grown on IV–VI substrates which are expensive and generally less robust than Si sub-

Manuscript received March, 2, 1998; revised May 28, 1998. This work was supported by the National Science Foundation through the EPSCoR program under Grant EPSCoR-92-OU.

M. F. Khodr is with Halliburton Energy Services, Fort Worth, TX 76140 USA.

P. J. McCann is with the School of Electrical and Computer Engineering and the Laboratory for Electronic Properties of Materials, University of Oklahoma, Norman, OK 73019 USA.

B. A. Mason is with the Department of Physics and Astronomy and the Laboratory for Electronic Properties of Materials, University of Oklahoma, Norman, OK 73019 USA.

Publisher Item Identifier S 0018-9197(98)06249-6.

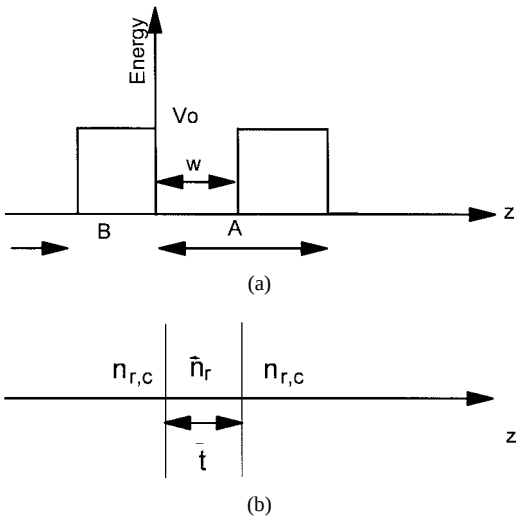

Fig. 1. (a) Periodic potential wells (Kronig–Penny model). The potential is periodic in z of period A with the barrier height V_o, barrier width B, and well width w. (b) Schematic representation of in a symmetric double-heterojunction waveguide. The refractive indices for the active region and the cladding layers are shown along with the thickness of the active region.

strates. To take advantage of the developed VLSI technology in Si, researchers are investigating the fabrication of IV–VI QW devices on Si substrates [6]. However, most of the IV–VI materials have higher lattice constants and thermal expansion coefficients than silicon. None of these factors is a significant limitation when interposing BaF_2–CaF_2 insulating layers are introduced between the IV–VI materials and a silicon substrate [7]–[9].

Based on Kane's two-band model, a theoretical model was developed that finds the gain-current density relation in EuSe–PbSeTe IV–VI semiconductor single-quantum-well (SQW) lasers [10], [11]. EuSe was the barrier material and PbSeTe was the well material. This lattice-matched structure is of interest because it is also lattice-matched with BaF_2, a promising buffer material for growth of IV–VI semiconductors on silicon substrates [9]. The theoretical development is based on those formulas developed in the literature for the III–V semiconductors with the necessary modifications required for the IV–VI material systems. In these modifications, we included the effects of the anisotropy of the effective masses and the nonparabolicity of the bands. This model can also be used for other IV–VI material systems.

In previous publications, we studied the physical properties of IV– VI QW lasers of a SQW EuSe–$PbSe_{0.78}Te_{0.22}$–EuSe laser structure at a temperature of 77 K [10], [11]. To engineer these devices, MQW structures were studied to improve the gain–current density relation obtained in the SQW structure [10], [11]. In this paper, the MQW structure under study is shown in Fig. 1(a) where the well material is $PbSe_{0.78}Te_{0.22}$, the barrier material is EuSe, and the cladding material is the barrier material itself. The refractive index of the well material and barrier material are $n_{r,w}$ and $n_{r,B}\,(=n_{r,c})$, respectively.

We studied the amount of optical energy that is confined in this structure, the total losses, and the threshold current behavior as a function of laser cavity length and mirror reflectivity. The various effects of nonparabolicity of the bands on the design process are included in this presentation along with the theoretical formulation.

II. Energy Broadening in EuSe–PbSeTe MQW Structure

In a QW structure, a series of quantized energy levels and associated subbands are formed due to the confinement of electrons in the direction of the QW thickness. The MQW structures constitute a periodic array of potential wells or SQW's. The potential is periodic in z of period A, as shown in Fig. 1(a), with the barrier height V_o, barrier width B, and well width w. If a MQW structure is used instead of the SQW, each single energy level splits into a number of different energy levels. The difference between the top energy level and the bottom energy level in a single subband at $k_{\rm II}=0$ is referred to as the energy broadening (ΔE). The degree of energy broadening (ΔE) depends on the barrier height and thickness.

The coupling is important for obtaining a uniform carrier distribution in the MQW structure. However, strong coupling leads to the reduction in the two-dimensional (2-D) character of the well through smearing of the configuration of the density of states. In order to obtain good uniformity of carrier concentration and maintain the 2-D properties of the well, the following relations are required [2], [12]:

$$\hbar/\tau_r \ll \Delta E \ll \hbar/\tau_{\rm in}$$

where τ_r is the carrier recombination time at lasing and $\tau_{\rm in}$ is the intraband relaxation time. Inserting an approximate value for $\tau_r \approx 3\text{-}4\times10^{-9}$ s and $\tau_{\rm in} \approx 2.3\times10^{-12}$ s, a value of $\Delta E \leq 1$ meV is sufficient to fulfill the above condition [13].

The calculations of the energy broadening ΔE can be done using the simple one-dimensional Kronig–Penny equation which was derived in the envelope wave function approximation, using the Kane model to describe the band structure within each well and barrier [14]. In this reference, Bastard and Brum have shown that for the transverse electron wavevector $k_\perp = 0$ in the parabolic band approximation, the equation yielding the values of ΔE takes the simple Kronig–Penny form

$$\cos kA = \frac{1}{2}(1/\xi - \xi)\sin kw \sinh \kappa B + \cos kw \cosh \kappa B \quad (1)$$

with $\xi = m_b^* k/m_w^* \kappa$, $k^2 = 2m_w^* \varepsilon_n/\hbar^2$, and $\kappa^2 = 2m_b^*(V_o - \varepsilon_n)/\hbar^2$. The symbols m_w^* and m_b^* are the effective masses inside and outside the well, respectively. The wavevectors k and κ are parallel to the direction of the well (the growth direction). The subscript that denotes the parallel direction is dropped for simplicity.

To calculate the values of ΔE for nonparabolic bands, the energy-dependent effective mass approach can be directly applied to the above equation by replacing the well effective mass or band edge mass in the z-band model m_w^* by the energy-dependent effective mass [10], [11]

$$m_w^*(E_z) = m_w^*(1 + 2E_z/E_g) \quad (2)$$

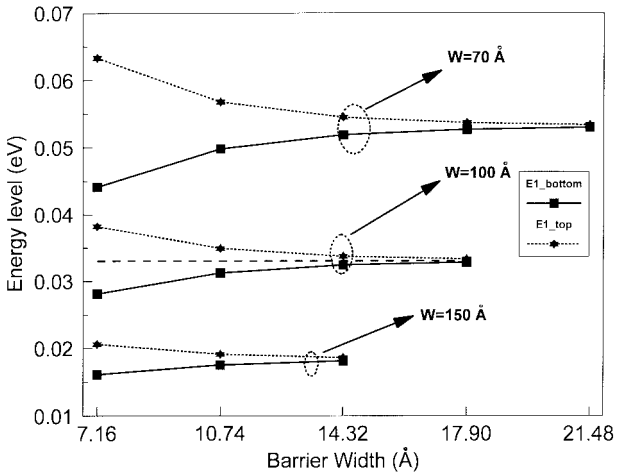

Fig. 2. The top and bottom of the first energy band for the parabolic system as a function of barrier width. The dashed line for the 100-Å well represents the discrete energy level.

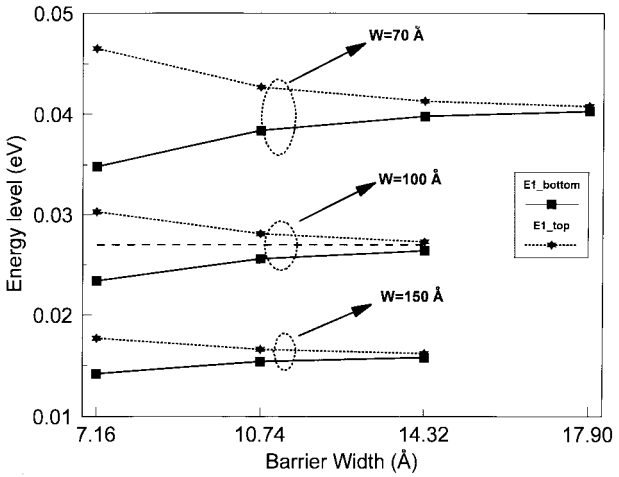

Fig. 3. The top and bottom of the first energy band for the nonparabolic system as a function of barrier width. The dashed line for the 100-Å well represents the discrete energy level.

where $E_z(k)$ is the energy dispersion in the z direction in the unperturbed periodic lattice [10], [11]

$$E_z = -\frac{1}{2}E_g \pm \sqrt{\frac{1}{4}E_g^2 + \frac{\hbar^2 E_g}{2m_w^*}k^2} \tag{3}$$

and E_g is the bandgap energy.

The EuSe–$PbSe_{0.78}Te_{0.22}$ MQW structure proposed has a periodic potential in z of period $A = w + B$ [Fig. 1(a)]. The well material is $PbSe_{0.78}Te_{0.22}$ and the barrier material is EuSe with 77 K bandgaps of 0.2 and 1.8 eV [15], respectively. The well growth is in the [100] direction and it is assumed that the discontinuities in the conduction band and valence band edges are equal. This assumption is valid based upon work by Partin [6] and Yuan *et al.* [16]. A barrier height is $V_o = 0.8$ eV, the effective mass in the well is $m_w^* = 0.05m_o$, and the effective mass in the barrier is $m_b^* = 0.4m_o$ [10].

The solutions for the first energy subband using (1) and neglecting the effects of nonparabolicity of the bands are shown in Fig. 2 for three different well widths of 70, 100, and 150 Å. The bottom energy levels of the first subband are depicted with solid lines and the top levels of the first subband with dotted lines. Since EuSe is face-centered cubic, the increment value of the barrier width is equal to the spacing between the {100} planes, a value of 3.10 Å [17]. From the figure, the bottom and the top energy levels approach each other as the barrier width increases. This difference, which is referred to as band broadening, has a maximum allowed value of 1 meV, as required. The barrier thickness value at which ΔE is less than or equal to 1 meV will be called the minimum barrier thickness ($B_{\min}$). These minimum thickness values will be needed when we discuss the MQW structures. In addition, this energy broadening decreases as the well width increases at a fixed barrier width because the electrons occupy lower energy levels and thus the wavefunctions do not overlap strongly with neighboring wells. Increasing the barrier width above $B_{\min}$ leads eventually to the discrete energy levels for the SQW which are independent of B. The dashed line for well width $w = 100$ Å represents the first discrete energy level as calculated for the SQW structure [10], [11] (see Fig. 3).

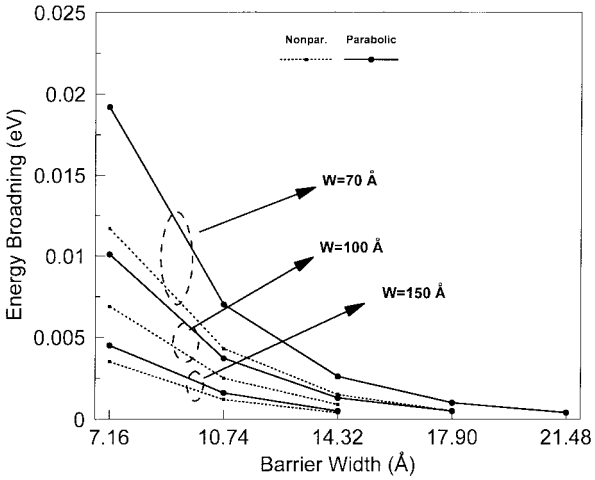

Fig. 4. The first energy band broadening for the parabolic and nonparabolic systems as a function of barrier width.

The calculations for the energy broadening, including the effects of nonparabolicity in the bands, as a function of the barrier width were performed using (1) and the energy-dependent effective mass (2). The data in the figures reveal a similar behavior to that seen above for the parabolic case. However, from Fig. 4, the energy broadening including the effects of nonparabolicity in the bands is less than its parabolic counterpart while the values for $B_{\min}$ are equal for both cases. The difference in energy broadening between the two cases can be explained following the same reasoning as above for the wide well effects. Lowering the occupied energy levels of the electrons confined in the well results in smaller coupling effects. The effects of nonparabolicity on the minimum barrier thickness are not important for this system due to the large barrier increment. In addition, the effects of nonparabolicity are not obvious for the 150-Å—wide well because of its negligible effects on the energy levels in wide wells.

Finally, the value of B at a fixed well width should be chosen such that ΔE satisfies the inequality above. For $w =$

100 Å, the well width of interest in this work, the values ($B_{\min}$) were found to be equal to 15.5 Å for both the parabolic and nonparabolic bands. The thicker the well, the thinner the barrier needed to keep $\Delta E \leq 1$ meV. Therefore, a barrier thickness value greater than $B_{\min}$ ensures that $\Delta E \leq 1$ meV. A barrier thickness value of 25 Å was found to be greater than $B_{\min}$ for well width values $w \geq 100$ Å. This barrier thickness value is used in the forthcoming analysis.

III. Calculations of the Optical Confinement Factor

The optical confinement factor depicts the overlap of the optically guided wave with the quantum well, according to the formula

$$\Gamma_o = \frac{\int_{-w/2}^{w/2} E_o^2(z)\,dz}{\int_{-\infty}^{+\infty} E_o^2(z)\,dz} \tag{4}$$

where $E_o(z)$ is the electrical field intensity of the first transverse mode (TE_o) propagating in the active region. In other words, this formula defines the fraction of the mode energy which is confined to the active layer and thus "sees" optical gain [18].

The optical analysis of SQW lasers is conventional in that one solves for the TE modes in a three-region dielectric optical waveguide [18]. A planar SQW structure is commonly represented as a three-layer slab dielectric waveguide where the guiding layer corresponds to the active layer and the cladding layers correspond to the passive layers. If the structure is symmetrical, i.e., the cladding layers have the same index of refraction, then the waveguide will always support at least one propagation mode [18]. Fig. 1(b) depicts such a SQW structure for which $\overline{n}_r\,(=n_{r,w})$, $n_{r,c}\,(n_{r,w} > n_{r,c})$ are the indices of refraction of the active and cladding layers, respectively, and $\overline{t} = w$ is the thickness of the active layer. In practice, w is so small that only the fundamental transverse mode lases. It is also found experimentally that its polarization is almost invariably TE [18]. For these reasons, one is mostly concerned with the propagating characteristics of the TE_o mode in a symmetrical slab guide. A more general approximate solution for (4) that is valid for all w is found by Botez [19], [20]. Botez's analytical techniques yield quite accurate results in calculating Γ_o for three-region dielectric guides [19]. The analytical approximation given by Botez for calculating the optical confinement factor Γ_o in a symmetrical waveguide for the TE_o mode is

$$\Gamma_o \cong \frac{D^2}{D^2+2} \tag{5}$$

where

$$D = 2\pi\left(\frac{w}{\lambda}\right)\sqrt{(n_{r,w}^2 - n_{r,c}^2)}. \tag{6}$$

λ is the vacuum wavelength at the lasing photon energy and D is the normalized thickness of the active region.

Plotting the confinement factor as a function of well width in Fig. 5 for the EuSe–$PbSe_{0.78}Te_{0.22}$ SQW structure shows that Γ_o decreases with decreasing w. The photon energy emitted

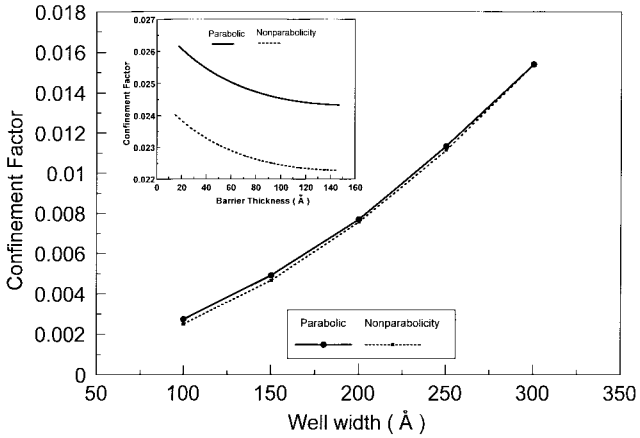

Fig. 5. The optical confinement factor as a function of well width for the EuSe–$PbSe_{0.78}Te_{0.22}$ MQW structure. The inset shows the optical confinement factor as a function of barrier thickness for the structure where the well width is 100 Å and the number of wells N_w is 3.

is itself a function of well width in QW lasers because of the dependence of the quantized energy levels on w. This shift of the photon energy or wavelength affects the value of the index of refraction of the well material. In this work, these variations of the index of refraction with emitted photon wavelength are not considered. Because of only recent interest in this material system, these data are not currently available. Therefore, the index of refraction of the well material is fixed at $n_{r,w} = 6$ [21] and that of the cladding layer at $n_{r,c} = 2.43$ [22]. From this figure, the nonparabolicity of the bands decreases the value of Γ_o at smaller well widths. This is expected because including the nonparabolicity for this system shifts the energy levels toward the band extrema and thus increases the emitted photon wavelength λ which decreases Γ_o, as seen from (5).

The calculations of the confinement factor for a MQW structure like the one shown in Fig. 1(a) can be found considering the structure as a three-region waveguide with identical cladding layers (same $n_{r,c}$), plus a center layer of average thickness $\overline{t}$ and average index of refraction $\overline{n}_r$ [23]. These average quantities for the MQW structures are given by the following equations [23]:

$$\overline{t} = N_w w + N_B B \tag{7}$$

and

$$\overline{n}_r = \frac{N_w w n_{r,w} + N_B B n_{r,B}}{\overline{t}} \tag{8}$$

where N_w and N_B are the number of wells and barriers, respectively, whereas w and B are their thicknesses. The confinement factor for these structures is given by [23]

$$\Gamma_o^M = \Gamma_o \frac{N_w w}{\overline{t}} \tag{9}$$

where Γ_o is given in (5) with $D \to \overline{D}$

$$\overline{D} = 2\pi\left(\frac{\overline{t}}{\lambda}\right)\sqrt{(\overline{n}_r^2 - n_{r,c}^2)}. \tag{10}$$

The three-region waveguide with $n_{r,c}$, $\overline{n}_r$, and $\overline{t}$ is an accurate model for a MQW laser when the waveguide supports only the

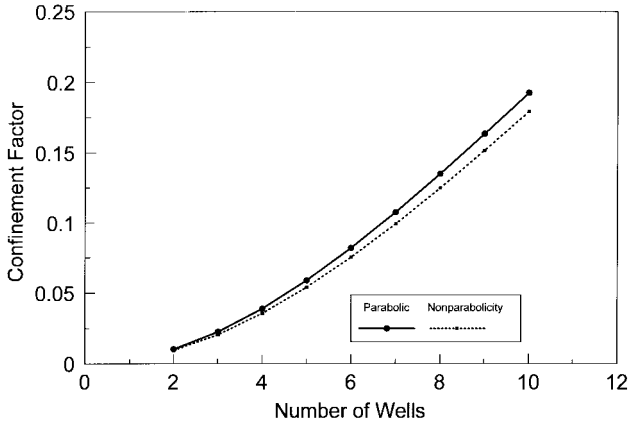

Fig. 6. The optical confinement factor as a function of the number of wells for the EuSe–$PbSe_{0.78}Te_{0.22}$ MQW structure where the well width is 100 Å.

fundamental mode, and the model decreases in accuracy as the device parameters are modified such that higher order modes propagate [23].

The above formulas are used to calculate the confinement factor for EuSe–$PbSe_{0.78}Te_{0.22}$ MQW structures where $w = 100$ Å. The well material $PbSe_{0.78}Te_{0.22}$ index of refraction is $n_{r,w} = 6$. The barrier material is EuSe with an index of refraction $n_{r,B} = 2.43$ and a minimum barrier thickness $B_{\min} = 25$ Å, as found in Section II.

The confinement factor, as a function of the number of wells for the parabolic system and for the nonparabolic system, is shown in Fig. 6. From this figure, Γ_o^M increases with the number of wells and its values for the parabolic case are higher than its values for the nonparabolic case for the same reasons mentioned above for the SQW structure.

The above analysis was done at a fixed barrier thickness value of 25 Å. However, the values of the confinement factor depend on the barrier thickness values through (7) and (8). Increasing the barrier thickness above $B_{\min}$, the confinement factor decreases as seen from the inset of Fig. 5 for the parabolic and nonparabolic bands. The values of Γ_o^M shown in this figure are for a well width $w = 100$ Å, $n_{r,B} = 2.43$, $n_{r,c} = 1.46$, $N_w = 3.0$, and $N_B = N_w - 1$. The drop in Γ_o^M for $B > B_{\min}$ is faster for thinner barriers than for thicker ones. Therefore, designing a MQW with barrier thickness values that are comparable to the well width values reduces the confinement factor from that at $B_{\min}$. Further increase in the barrier thickness value does not have a big effect on the confinement values, as shown in the inset of Fig. 5. On the other hand, the confinement factor values for MQW design structures are higher and more sensitive to the variations in thickness values for thinner barriers.

IV. Calculations of Total Losses

The total losses are given by the relation [26]

$$\alpha_{\text{total}} = \Gamma_o^{\text{QW}}\alpha_{\text{fc}} + \alpha_s + \frac{1}{2L}\ln\frac{1}{R_1R_2} \tag{11}$$

where α_{fc} is the free carrier absorption, Γ_o^{QW} is the confinement factor, and α_s is the scattering loss due to waveguide imperfections. The loss due to radiation from the ends of the laser is given by

$$\alpha_c = \frac{1}{2L}\ln\frac{1}{R_1R_2} \tag{12}$$

where L is the laser cavity length and R_1 and R_2 are the end facet reflectivities.

Free carrier absorption is crucial to semiconductor lasers because it is a major unavoidable loss mechanism. It results from the scattering of carriers in motion and is therefore influenced by the same scattering mechanisms that influence carrier mobility [26]. An expression for free carrier absorption in lead salts has been given by Anderson [27]

$$\alpha_{\text{fc}} = \frac{N_n e^3}{n_r c\varepsilon_o \mu_n (m_w^*)^2(\hbar\omega)^2} \tag{13}$$

where N_n is the carrier concentration, μ_n is the carrier mobility, $\hbar\omega$ is the emitted photon energy, and m_w^* is the conductivity effective mass in the active region. The constants e, c, and ε_o are the electron charge, speed of light, and permittivity of free space, respectively. Typical values of the carrier concentrations and mobilities in $PbSe_{0.78}Te_{0.22}$ films are $\cong 10^{17}$ cm^{-3} and $\cong 10^4$ cm^2·V^{-1} · s^{-1} at 77 K [15]. Substituting these values and $n_r = 6.0, m_w^* = 0.05$, and $\hbar\omega = 0.2$ eV into (13), we calculate the free carrier absorption value $\alpha_{\text{fc}} \cong 1.3$ (1/cm). This is a small loss value when multiplied by the confinement factor for a QW structure (typical value of $\cong 0.03$), thus the first term in (11) can be neglected. Therefore, the losses due to free carrier absorption in QW structures are negligible, mainly because of the small confinement factor [18].

The scattering loss α_s is due to scattering of radiation out of the optical waveguide by either nonplanar heterostructure interfaces or imperfections in the dielectric layers [26]. Several mathematical models of discrete and continuous waveguide deformations from which optical scattering losses were computed as functions of parameters which characterize the severity of the imperfection can be found in [28]. Here, however, we assume a defect-free interface layer, thus $\alpha_s = 0$ and the second term in (11) is neglected. Because of the small loss values of the first and second terms of (11), it is reasonable to neglect these two terms in our model.

V. Modal Gain–Current Density Calculations

The analytic form for the maximum gain and current density expressions in IV–VI SQW lasers are discussed in depth and given in [11]. However, in laser oscillators, the important design parameter is the modal gain rather than the maximum gain. It is defined as the gain experienced by the traveling laser mode [1]. It is obtained by multiplying the maximum gain values by the confinement factor. In order for laser oscillation to occur, the modal gain at the lasing photon energy $\hbar\omega_1$ must be equal to the total losses α_{total}. The laser oscillation condition is given as [26]

$$g_{\text{mod}}(\hbar\omega_1) = \alpha_{\text{total}}. \tag{14}$$

The current density that corresponds to this modal gain value is the threshold current density (J_{th}).

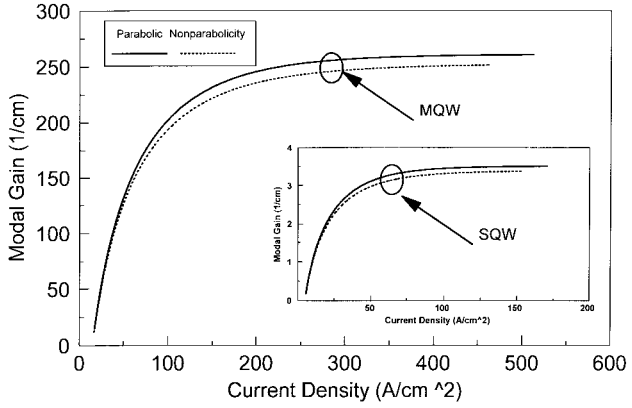

Fig. 7. The modal gain as a function of current density for the EuSe–$PbSe_{0.78}Te_{0.22}$ MQW structure (at 77 K). The well width is 100 Å and the number of wells is 3. The inset shows the modal gain as a function of current density for the EuSe–$PbSe_{0.78}Te_{0.22}$ SQW structure (at 77 K) where the well width is 100 Å.

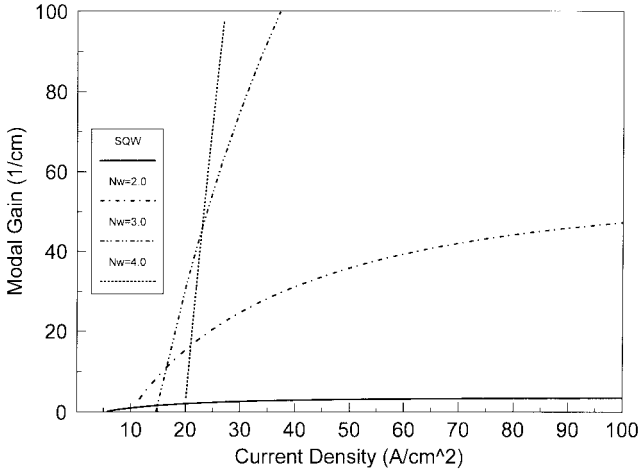

Fig. 8. The modal gain as a function of current density for the nonparabolic EuSe–$PbSe_{0.78}Te_{0.22}$ SQW and MQW structures (at 77 K) with the number of wells equal 2, 3, and 4. The well width is 100 Å in all the structures.

The modal gain and current density calculations for the EuSe–$PbSe_{0.78}Te_{0.22}$–BaF_2 SQW structure where $w = 100$ Å are shown in the inset of Fig. 7. The SQW curve reflects the fact that SQW laser structures are suitable for low-loss applications [11]. On the other hand, the EuSe–$PbSe_{0.78}Te_{0.22}$ MQW structure is suitable for high loss applications, as noted in Fig. 7 for a $N_w = 3.0$. The high modal gain values in this structure are due to the high confinement factor values shown in Fig. 5. Similar to the SQW structure, the nonparabolicity of the bands shifts the gain–current density to the left of the parabolic curve, reducing the modal gain and increasing the current density at some fixed gain value.

In Fig. 8, a comparison is made between the modal gain and current density values for the SQW and the MQW where $N_w = 2$, 3, and 4. The modal gain region of interest is between 0 and 100 cm^{-1} because of the cross over points between the different structures. From this figure it is noted that, for low losses, the injected threshold current density is minimal in the case of SQW structures. If $11 < \alpha_{\text{total}} < 45$ cm^{-1}, the threshold current density for the three-well structure is lower

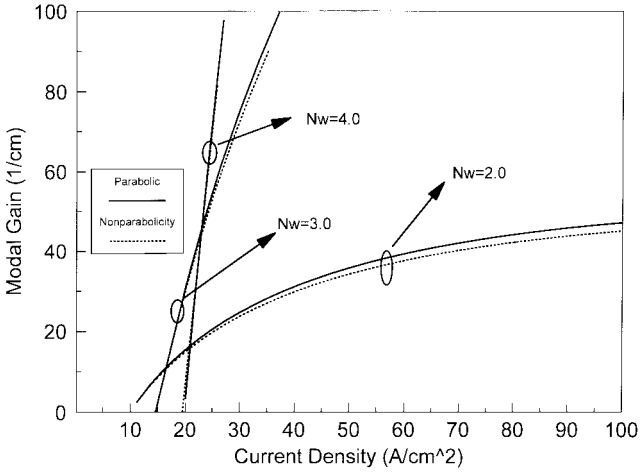

Fig. 9. The modal gain as a function of current density for the EuSe–$PbSe_{0.78}Te_{0.22}$ MQW structures (at 77 K) with number of wells as a parameter. The well width is 100 Å.

than that of the two-well structure. At higher values of α_{total}, which call for large laser modal gain, a larger number of wells are needed. It is also noted that for $\alpha_{\text{total}} > 45$ cm^{-1}, a four-well structure ($N_w = 4$) will have the lowest threshold current density. The curves shown in Fig. 9. illustrate that including the effects of nonparabolicity of the bands reduces the cross over α_{total} values below those obtained for the parabolic bands. From this figure, these effects are noticed to be small.

VI. Threshold Current Calculations

The current needed to compensate for the total loss α_{total} (11) is called the threshold current (I_{th}) and is calculated by the usual formula [26]

$$I_{\text{th}} = J_{\text{th}} \times \text{Area} \tag{15}$$

where the Area of the QW equals $L\times$ width. The threshold current density (J_{th}) corresponds to the modal gain value that satisfies the oscillation condition ($\alpha_{\text{total}} = g_{\text{mod}}(\hbar\omega_l)$) and can be obtained from the modal gain–current density plots. The threshold current calculations are performed assuming the width has a constant value of 1 μm, the cavity length L as an independent variable L, and the mirror reflectivities as a parameter. The total losses are calculated using (11) where the free carrier loss and the scattering loss terms are neglected.

The threshold current–cavity length relations for the EuSe–$PbSe_{0.78}Te_{0.22}$ MQW structure are shown in Fig. 10. The number of wells for both structures $N_w = 3$ is considered a satisfactory one for the current analysis because of the high modal gain values. The threshold current calculations for the MQW structure are performed using (11) and Fig. 7. The reflectivity at one end R_1 is fixed at some value and the reflectivity at the other end R_2 is 0.5, 0.7, and 0.9. From these plots, one notices that each curve has a minimum threshold current value at a critical cavity length. Increasing the reflectivity factor R_1R_2 decreases the threshold current values and the critical cavity length. This behavior is seen in thin QW lasers [29], [30]. The region above the critical thickness value corresponds to the low modal gain regime (or

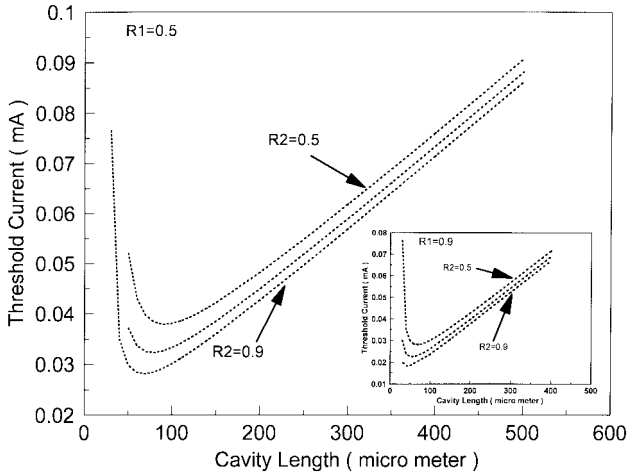

Fig. 10. The threshold current as a function of cavity length for the nonparabolic EuSe–$PbSe_{0.78}Te_{0.22}$ MQW structure (at 77 K) with R_2 as a parameter and R_1 fixed at 0.5. In the inset R_1 is fixed at 0.9. The well width is 100 Å and the number of wells is 3.

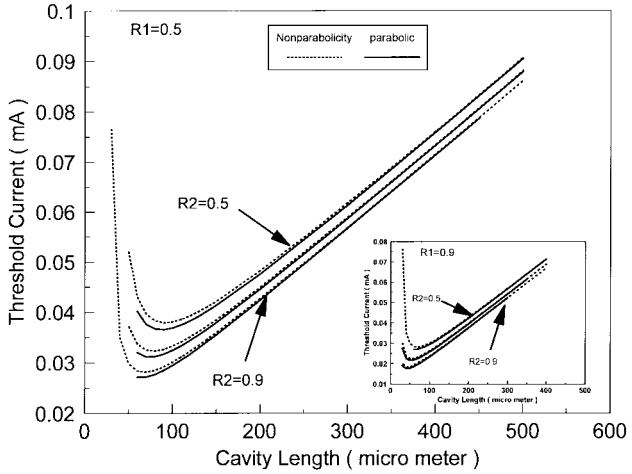

Fig. 11. The threshold current as a function of cavity length for the EuSe–$PbSe_{0.78}Te_{0.22}$ MQW structure (at 77 K) with R_2 as a parameter and R_1 fixed at 0.5. In the inset R_1 is fixed at 0.9. The well width is 100 Å and the number of wells is 3.

low losses regime) where $I_{\rm th} \propto L$. However, the region below the critical cavity length value corresponds to the high modal gain regime (or high losses regime) where the modal gain increases more slowly with J than at lower values of $g_{\rm mod}$ [30].

The effects of nonparabolicity of the bands on the threshold current are illustrated in Fig. 11. From the previous section, the effects of nonparabolicity on the modal gain–current density relation are to shift the modal gain–current density curve down and to the right of the parabolic reference curve. These effects are more noticeable in the high-gain regime (or high-loss regime) than in the low gain regime (or low loss regime), Fig. 7. Therefore, for a fixed total loss value in the low-loss regime, the effects of nonparabolicity on the threshold current values are very small. Increasing the total loss by decreasing L or R_1R_2, these effects become more and more pronounced, as shown in Fig. 11. For a QW laser, a typical cavity length value of 250 μm is usually used. At this typical value, the effects of nonparabolicity on the threshold current values can be neglected without loss of accuracy. What is not to be neglected is the 20% shift in the output lasing energy.

The small threshold current values calculated for the above structures could be due to the assumption made earlier that the internal quantum efficiency is one. In other words, we neglected the nonradiative contributions to the current that come from the thermal leakage of the carriers over the confining potential barriers and from the Auger recombination. The first energy level for the EuSe–$PbSe_{0.78}Te_{0.22}$ QW of width w =s 100 Å was found to be 0.033 eV assuming parabolic bands and 0.026 eV assuming nonparabolic bands. Thus, the thermal energy needed to overcome the potential barrier is 0.767 eV assuming parabolic bands and 0.774 assuming nonparabolic bands, knowing that barrier potential for our system is $V_o = 0.8$ eV. The thermal energy (kT) of the carriers at 77 K is $\equiv$ 0.007 eV, which is not enough to overcome this high barrier. Based on this simple argument, the contribution from the leakage current can be considered negligible. The contributions to the current due to Auger recombination are left for future work and are not addressed here. The calculations that lead to the evaluation of the internal quantum efficiency will help determine the external quantum efficiency and the output power from these devices.

Finally, the above structures can be grown on a fluoride buffer layer grown on a Si substrate. The fluoride buffer layer can be composed of a BaF_2 layer which is lattice matched to EuSe on top of a **CaF_2** layer which is approximately lattice-matched to a Si substrate. In addition, these fluoride layers are useful as an antireflection coatings in optically pumping these structures [31]. Also, the BaF_2layer can be used to modify the MQW structure to the MMQW structure. Details of the above applications can be found in [31].

VII. Conclusion

We used the 100-Å well in studying the effects of adding more than one well on the energy broadening of the first excited state. This investigation was performed using the Kronig–Penny model for the EuSe–$PbSe_{0.78}Te_{0.22}$ system with parabolic and nonparabolic bands. The nonparabolic effects were studied using the energy-dependent-effective-mass method. The theoretical model solves for the confinement factor, total losses, modal gain–current density relation, and theoretical current for the MQW quantum structure. In this structure, the minimum barrier thickness values that are needed to minimize the coupling between the wells can be calculated using the Kronig–Penny model for the nonparabolic bands using the energy-dependent-effective-mass equation. This is important for any design of a MQW structure in order to obtain good uniformity of carrier concentration and maintain the 2-D properties of the well.

The nonparabolicity of the bands in the growth direction lowers the values of the confinement factor relative to those for the parabolic bands which in turn lowers the modal gain values. The calculated modal gain values for the MQW structure increase with an increase in the number of wells. At low modal gain values, there are crossover points between the

gain–current density curves. These crossover points depend on the number of wells. Increasing the number of wells causes the gain–current density curves to be steeper and the minimum current density value to increase. The effects of nonparabolicity on these cross over points are small because they fall in the low gain region. However, these effects are more noticeable at the high gain region and close to saturation.

The threshold current as a function of cavity length with mirror reflectivity as a parameter was obtained for the MQW structure. In each curve, the threshold current decreases with a decrease in the cavity length and then increases at a critical cavity length. The critical cavity length and the corresponding threshold current value are smallest for the highest mirror reflectivity values. The effects of nonparabolicity on the threshold current values are more obvious for short cavities and decrease with an increase in cavity length. Short cavities mean high losses and long cavities mean small losses. Thus, in terms of the modal gain–current density curves, the modal gain values needed to overcome the high losses are close to the gain saturation level. At these high gain levels, the effects of nonparabolicity are obvious. On the other hand, the modal gain values needed to overcome the small losses are closer to the lower gain level. At this gain level, the effects of nonparabolicity are less obvious.

Whether the SQW or the MQW is the better structure depends on the loss level. At low loss, the SQW laser is always better because of its lower current density where only one QW has to be inverted. At high loss, the MQW is always better because the phenomena of gain saturation can be avoided by increasing the number of QW's (N_w) although the injected current to achieve this maximum gain also increases by N_w. Owing to this gain saturation effect, there exists an optimum number of QW's for minimizing the threshold current for a given total loss α_{total}. At this typical value, the effects of nonparabolicity on the threshold current values can be neglected without loss of accuracy. However, there is a 20% shift in the output lasing energy that cannot be neglected.

REFERENCES

[1] S. R. Chinn, P. S. Zory, and A. R. Reisinger, "A model for GRIN-SCH-SQW diode lasers," *IEEE J. Quantum Electron.*, vol. 24, pp. 2191–2214, 1988.

[2] Y. Arakawa and A. Yariv, "Quantum well lasers-gain, spectra, dynamics," *IEEE J. Quantum Electron.,* vol. QE-22, pp. 1887–1898, 1986.

[3] T. H. Wood, C. A. Burrus, D. A. B. Miller, D. S. Chemla, T. C. Damen, A. C. Gossard, and W. Wiegmann, "High-speed optical modulation with GaAs/GaAlAs quantum wells in p-i-n diode structure," *Appl. Phys. Lett.*, vol. 44, p. 16–18, 1984.

[4] D. A. B. Miller, D. S. Chemla, T. C. Damen, A. C. Gossard, W. Wiegmann, T. H. Wood, and C. A. Burrus, "Novel hybrid optically bistable switch: The quantum well self-optic effect device," *Appl. Phys. Lett.,* vol. 45, pp. 13–15, 1984.

[5] K. Hess, B. A. Vojak, N. Holonyak, Jr., and R. Chin, "Temperature dependent of threshold current for a quantum-well heterostructure lasers," *Solid-State Electron.,* vol. 23, pp. 585–589, 1980.

[6] D. L. Partin, "Lead salt quantum effect structures," *IEEE J. Quantum Electron.,* vol. 24, pp. 1716–1726, 1988.

[7] M. Wittmer, D. A. Smith, A. Segmüller, H. Zogg, and H. Melchior, "Characterization of epitaxial (Ca, Ba)F_2 films on Si(111) substrates," *Appl. Phys. Lett.,* vol. 49, pp. 898–900, 1986.

[8] H. Zogg, P. Maier, and H. Melchior, "Graded IIa-fluoride buffer layers for heteroepitaxy of lead-chalcogenides and CdTe on Si," *J. Cryst. Growth,* vol. 80, pp. 408–416, 1987.

[9] H. Zogg, "Strain relief in epitaxial fluoride buffer layers for semiconductor heteroepitaxy," *Appl. Phys. Lett.*, p. 49, 993–995, 1986.

[10] M. F. Khodr, P. J. McCann, and B. A. Mason, "Gain and current density calculation in IV–VI quantum well lasers," *J. Appl. Phys.,* vol. 77, pp. 4927–4930, 1995.

[11] ———, "Effects of band nonparabolicity on the gain and current density in EuSe–$PbSe_{0.78}Te_{0.22}$–$EuSe$ IV–VI semiconductor quantum well lasers," *IEEE J. Quantum Electron.,* vol. 32, pp. 236–247, 1996.

[12] A. Yariv, C. Lindsey, and U. Sivan, "Approximate analytic solution for electronic wave functions and energies in coupled quantum wells," *J. Appl. Phys.,* vol. 58, pp. 3669–3671, 1985.

[13] M. Asada, A. Kameyamaan, and Y. Suematsu, "Gain and intervalence band absorption in quantum-well lasers, *IEEE J. Quantum Electron.,* vol. QE-20, pp. 745–753, 1984.

[14] G. Bastard and J. A. Brum, "Electronic states in semiconductor heterostructures," *IEEE J. Quantum Electron.,* vol. QE-22, pp. 1625–1644, 1986.

[15] P. J. McCann and C. G. Fonstad, "$PbSe_{0.78}Te_{0.22}$ lattice-matched with BaF_2," *Thin Solid Films,* vol. 27, pp. 185–189, 1993.

[16] S. Yuan, H. Krenn, G. Springholz, and G. Bauer, "Large refractive index enhancement in PbTe/$Pb_{1-x}Eu_xTe$ multiquantum-well structures," *Appl. Phys. Lett.,* vol. 62, pp. 885–887, 1993.

[17] J. W. Mayer and S. S. Lau, *Electronic Materials Science: For Integrated Circuits in Si and GaAs.* New York: Macmillan, 1990.

[18] C. Weisbuch and B. Vinter, *Quantum Semiconductor Structures: Fundamentals and Applications.* San Diego, CA: Academic, 1991.

[19] D. Botez, "Analytical approximation of the radiation confinement factor for the TE_0 mode of a double heterojunction laser," *IEEE J. Quantum Electron.,* vol. QE-14, pp. 230–232, 1978.

[20] D. Botez, "Near and far-field analytical approximations for the fundamental mode in symmetrical waveguide DH lasers," *RCA Rev.,* vol. 39, pp. 577–603, 1978.

[21] P. K. Cheo, *Handbook of Solid-State Lasers.* New York: Marcel Dekker, 1989.

[22] J. B. Goodenough, A. Hammett, G. Uber, F. Hulliger, M. Leiß, S. K. Ramasesha, and H. Werheit, *Numerical Data and Functional Relationships in Science and Technology: New Series.* Berlin, Germany: Springer-Verlag, 1984.

[23] W. Streifer, D. R. Scrifres, and R. D. Burnham, "Optical analysis of multiple-quantum-well lasers," *Appl. Opt.,* vol. 18, pp. 3547–3548, 1979.

[24] M. J. Weber, *Handbook of Laser and Technology.* Boca Raton, FL: CRC Press, 1986.

[25] J. P. Noblanc, "Trends in quantum well devices," *Surf. Sci.,* vol. 168, pp. 847–851, 1986.

[26] H. C. Casey and M. B. Panish, *Heterostructure Lasers Part A: Fundamental Principles.* New York: Academic, 1978.

[27] W. W. Anderson, "Gain-frequency-current relation for $Pb_{1-x}Sn_xTe$ double heterostructure lasers," *IEEE J. Quantum Electron.,* vol. QE-13, pp. 532–543, 1977.

[28] F. R. Nash, W. R. Wagner, and R. L. Brown, "Threshold current variations and optical scattering losses in (Al, Ga)As double-heterostructure lasers," *J. Appl. Phys.,* vol. 47, pp. 3992–3994, 1976.

[29] P. L. Derry and A. Yariv, "Ultralow-threshold graded-index separate-confinement single quantum well buried heterostructure (Al, Ga)As lasers with high reflectivity coating," *Appl. Phys. Lett.,* vol. 50, pp. 1773–1775, 1987.

[30] P. S. Zory and A. R. Reisinger, "Anomalous length dependence of threshold for thin quantum well AlGaAs diode lasers," *Electron. Lett.,* vol. 22, pp. 475–476, 1986.

[31] M. F. Khodr, "IV–VI semiconductor quantum well lasers, physics and engineering," Ph.D. dissertation, University Microfilms Inc., MI, 1994.

M. F. Khodr, photograph and biography not available at the time of publication.

P. J. McCann, photograph and biography not available at the time of publication.

B. A. Mason, photograph and biography not available at the time of publication.